The C-terminus of Gain-of-Function Mutant p53 R273H Is Required for Association with PARP1 and Poly-ADP-Ribose

Devon Lundine[1,2], George K. Annor[1,2], Valery Chavez[1,2], Styliana Maimos[1], Zafar Syed[1], Shuhong Jiang[1], Viola Ellison[1], and Jill Bargonetti[1,2,3]

ABSTRACT

The TP53 gene is mutated in 80% of triple-negative breast cancers. Cells that harbor the hot-spot p53 gene mutation R273H produce an oncogenic mutant p53 (mtp53) that enhances cell proliferative and metastatic properties. The enhanced activities of mtp53 are collectively referred to as gain-of-function (GOF), and may include transcription-independent chromatin-based activities shared with wild-type p53 (wtp53) such as association with replicating DNA and DNA replication associated proteins like PARP1. However, how mtp53 upregulates cell proliferation is not well understood. wtp53 interacts with PARP1 using a portion of its C-terminus. The wtp53 oligomerization and far C-terminal domain (CTD) located within the C-terminus constitute putative GOF-associated domains, because mtp53 R273H expressing breast cancer cells lacking both domains manifest slow proliferation phenotypes. We addressed if the C-terminal region of mtp53 R273H is important for chromatin interaction and breast cancer cell proliferation using CRISPR-Cas9 mutated MDA-MB-468 cells endogenously expressing mtp53 R273H C-terminal deleted isoforms (R273HΔ381–388 and R273HΔ347–393). The mtp53 R273HΔ347–393 lacks the CTD and a portion of the oligomerization domain. We observed that cells harboring mtp53 R273HΔ347–393 (compared with mtp53 R273H full-length) manifest a significant reduction in chromatin, PARP1, poly-ADP-ribose (PAR), and replicating DNA binding. These cells also exhibited impaired response to hydroxyurea replicative stress, decreased sensitivity to the PARP-trapping drug combination temozolomide–talazoparib, and increased phosphorylated 53BP1 foci, suggesting reduced Okazaki fragment processing.

Implications: The C-terminal region of mtp53 confers GOF activity that mediates mtp53–PARP1 and PAR interactions assisting DNA replication, thus implicating new biomarkers for PARP inhibitor therapy.

Introduction

Wild-type p53 can regulate DNA replication

Wild-type p53 (wtp53) is well known for activating the transcription of target genes that control cell-cycle checkpoints (1). When the TP53 gene sustains hot-spot missense mutations in the DNA binding domain the mutant p53 (mtp53) protein does not perform transcription factor functions to induce growth arrest and apoptosis (1). The TP53 gene is mutated in 80% of triple-negative breast cancers (TNBC), the most aggressive subtype of breast cancer (2). Importantly, the missense mtp53 proteins expressed in cancers are highly stable and bind nonspecifically to DNA and tightly tether to chromatin (3). A lesser-known role of wtp53 is participation in regulation of DNA replication (3–5). wtp53 associates with cellular replicating DNA (4, 6). When associated with cellular genomes, wtp53 promotes DNA repair and influences the processivity of replication forks (independent of activating the transcription of p21 and inducing the G1/S checkpoint; refs. 7–10). In addition, p53 plays a direct role in recognition and repair of damaged DNA (11, 12). Studies report both wtp53 dependent increases and decreases in replication fork processivity, depending on variable study conditions. The mechanism of direct regulation of DNA synthesis by wtp53 does not require the N-terminal transactivation domain, however roles for the other 3 functional domains have yet to be rigorously examined (6, 13). Wtp53 and gain-of-function (GOF) mtp53 (found in tumors) share the same protein domains which include the N-terminal transactivation domain, the central site-specific DNA binding domain (which is mutated by one amino acid substitution in GOF mtp53), the adjacent oligomerization domain, and lastly a highly charged C-terminal domain (CTD) that interacts nonspecifically with DNA (3).

The C-terminus of wtp53 noncovalently interacts with poly-ADP-ribosylated PARP1

The proposed mechanism by which the C-terminus of wtp53 interacts with DNA is through a sliding clamp model (14). In the sliding clamp model, the CTD mediates fast sliding, while the central site-specific DNA binding domain associates with DNA and must hop from region to region. The C-terminus of wtp53 is also involved in other important interactions, one of which is association with PARP1 (15, 16). The p53 C-terminus interacts non-covalently with the poly-ADP-ribosylated (PARylated) PARP1 protein (17). When PARP1 associates with DNA damage its conformation is changed and the PARP protein moves on chromatin while sequentially PARylating itself, and histones, as it uses a "monkey bar" movement model (18). This chromatin interaction coupled with the enzymatic activity of PARP1 helps to safeguard the repair of lagging strand DNA replication (19, 20). A key function of PARP1 is to repair single strand gaps for

[1]The Department of Biological Sciences, Hunter College, Belfer Building, City University of New York, New York. [2]The Graduate Center Biology and Biochemistry Programs, City University of New York, New York. [3]Department of Cell and Developmental Biology, Weill Cornell Medical College, New York, New York.

D. Lundine and G.K. Annor contributed equally to this article.

Corresponding Authors: Jill Bargonetti, Hunter College, 413 East 69th Street, New York, NY 10021. Phone: 212-896-0465; E-mail: bargonetti@genectr.hunter.cuny.edu; and Viola Ellison, ve226@hunter.cuny.edu

Mol Cancer Res 2022;20:1799–810

doi: 10.1158/1541-7786.MCR-22-0133

Okazaki fragment processing, and PARP inhibition promotes cell death by increasing unrepaired DNA gaps (19, 21, 22). How the C-terminus of wtp53 and/or mtp53 might participate in the function of PARP1 gap suppression on replicating DNA is not yet understood. What is known is that GOF mtp53 R273H associates with PARP1 and replicating DNA (23).

mtp53 R273H interacts with replicating DNA and PARP1

A number of studies point to a potentially important connection between mtp53, PARP1, and PARP enzymatic activity in tumor cell survival. Several different methodologies have shown that GOF mtp53 R273H interacts with PARP1 and replicating DNA (3, 23–26). Loss of mtp53 R273H results in the reduction of several replication-associated proteins interacting with chromatin, including PARP1 and all 6 members of the replication helicase Mini Chromosome Maintenance (MCM) complex (24). Moreover, the increased interaction between mtp53 and replication machinery is recapitulated in tumors of genetically modified mice that express a GOF mtp53 analogous to mtp53 R273H (24). The human mtp53 R273H (in a number of different cell lines) resides in close proximity to both PARP1 and MCM proteins (23). Furthermore, high mtp53 expression associates with higher levels of PARylated proteins in cancer tissue (23). A strong positive correlation between high expression of mtp53 and PARP1 exists in the The Cancer Genome Atlas data set for breast cancers, and also in a small cohort of ethnically diverse breast cancer samples (23).

GOF mtp53 sensitizes breast cancer cells to PARP1 inhibitors

Blocking PARP1 activity with pharmacologic PARP inhibitors is standard protocol for breast cancers with BRCA1 mutations (27–29). Both loss of p53 function and GOF mtp53 expression sensitize cancer cells to PARP inhibition. Colon cancer HCT116 cells in a xenograft mouse model lacking wtp53 tumor suppressor function are more sensitive than their corresponding isogenic wtp53 counterpart to the PARP inhibitor Olaparib linked to a radio-ligand for delivery of targeted DNA damage (30). In addition, the expression of mtp53 increases the sensitivity of breast cancer cells to combination temozolomide and talazoparib treatment (23, 24). This increased sensitivity associates with reduced cell-cycle arrest, increased PARP1 trapping on chromatin, increased DNA damage and cell death (23, 24, 30).

Loss of the mtp53 C-terminus induces replication stress and reduces interaction with MCM proteins independent of oligomerization

The tetramerization of wtp53 is required for full tumor suppressor transcription function, but is not needed for mtp53 to associate with chromatin (31). We recently observed that MDA-MB-468 cell lines with mtp53 R273HΔ381–388 and mtp53 R273HΔ347–393 exhibit replication stress phenotypes (32). In addition, we detected that mtp53 R273HΔ347–393 no longer interacts well with chromatin or in close proximity to MCM proteins (31, 32). Deletion of the mtp53 R273H C-terminal amino acids Δ381–388, moderately disrupts mtp53 R273H replication function while a complete deletion of the mtp53 R273H C-terminal region, mtp53 R273HΔ347–393, causes more profound cellular changes (31, 32). As such, herein we examined if the C-terminal end of mtp53 R273H was required for the interaction with PARP1, poly-ADP-ribose (PAR), and replicating DNA. We found that endogenous expression of the C-terminal deletion mutant, mtp53 R273HΔ347–393, disrupted the protein's interaction with PARP1 and PAR, while also reducing the sensitivity to PARP inhibition, the response to hydroxyurea (HU)-induced replication stress and increased phosphorylated 53BP1 foci.

Materials and Methods

Materials

Solvents and chemicals were obtained from Sigma-Aldrich (St. Louis, MO, USA). DO1 p53 (catalog no. sc-126) monoclonal mouse, Actin (catalog no. sc-8432) monoclonal mouse, Lamin A (catalog no. SAB420042) monoclonal mouse, and PARP1 (catalog no. sc-7150) rabbit polyclonal antibodies were purchased from Santa Cruz (USA). Rabbit polyclonal antibodies against p53 (catalog no. 10442–1-AP) and PARP1 (catalog no. 13371–1-AP) were purchased from Proteintech. Additional antibodies against PARP1 were purchased from BD Biosciences (mouse monoclonal; catalog no. 51–6639GR) and Cell Signaling Technology (rabbit polyclonal; catalog no. 9532s). Anti—proliferating cell nuclear antigen (PCNA) mouse monoclonal (catalog no. NBP2–80905) was purchased from Novus Biologicals. Goat anti–rabbit-Cy5 (catalog no. PA45011), Goat anti–mouse-Cy3 (catalog no. PA43009) were purchased from Cytiva/Amersham. Antibodies used in the proximity ligation assay (PLA) and immunofluorescence were purchased from Sigma (PARP1, catalog no. PLA0184; 53BP1, catalog no. DUO92004; 53BP1^{Ser25}, catalog no. PLA 0126) and Cell Signaling Technology (PAR, catalog no. 83732) rabbit polyclonal. An Eppendorf 5415 refrigerated centrifuge was used for preparation of all extracts.

Cell culture

Human breast cancer cell line MDA-MB-468 (RRID:CVCL_0419) was purchased from ATCC (www.atcc.org) and the HCT116 (RRID: CVCL_S744) colon cancer cell line that is p53−/− was a gift from Bert Vogelstein (33, 34). Cells were routinely checked for mycoplasma contamination by PCR assay (ATCC) and maintained at 5% CO_2 in a 37°C humidified incubator in culture for ≤30 passages. HCT116 p53−/− and MDA-MB-468 cells were cultured in McCoy's 5A (Gibco) and DMEM media (Corning) respectively, with 50 U/mL penicillin, 50 μg/mL streptomycin (Mediatech), 5 μg/mL plasmocin (InvivoGen), and supplemented with 10% FBS (Gemini). CRISPR-Cas9 modified MDA-MB-468 cell lines expressing R273H variants Δ381–388, or Δ347–393, or *fs*387 were authenticated and verified as derivatives of MDA-MB-468 by IDEXX BioAnalytics (IDEXX BioAnalytics Case #39324–2021 completed 12/30/21).

Whole cell lysis and immunoblotting

Cells were harvested at 1,400 *g* (1,100 rpm) for 5 minutes at 4°C in Sorvall benchtop centrifuge. Cells were washed 3 times with ice-cold PBS and resuspended in RIPA buffer [0.1% SDS, 1% IGEPAL NP-40, 0.5% deoxycholate, 150 mmol/L NaCl, 1 mmol/L EDTA, 0.5 mmol/L EGTA, 50 mmol/L Tris-Cl pH 8.0, 1 mmol/L phenylmethylsulfonylfluoride (PMSF), 8.5 μg/mL Aprotinin, 100 μmol/L phosphatase inhibitor cocktail (Sigma), and 2 μg/mL Leupeptin]. The cell suspension was incubated on ice for 30 minutes to lyse the cells, vortexing every 5 minutes. Additional sonication of lysate for 3x for 30-second pulses/30-second rest on ice at 98% amplitude was done after the incubation. Samples were centrifuged at 15,700 *g* (13,200 rpm) for 30 minutes at 4°C, the supernatant collected, and protein quantified via Bradford Assay (Bio-Rad). Cell extracts were run on SDS-PAGE to separate samples followed by electro-blotting onto polyvinylidene fluoride membrane (GE Healthcare Amersham Biosciences). The membrane was blocked with 5% nonfat milk (Bio-Rad) in 1X PBS-0.1% Tween-20 followed by incubation with primary antibody overnight at 4°C. The membrane was washed 3x with 1X PBS-0.1% Tween-20 and incubated with Cy5 and Cy3-linked secondary antibodies for 1 hour at room temperature. The signal was detected with

the Typhoon FLA 7000 laser scanner (GE Healthcare). Quantification of Western blot signal was done by densitometry using ImageJ. Antibodies used were rabbit polyclonal antibodies against p53 (catalog no. 10442–1-AP) and monoclonal mouse against Actin (catalog no. sc-8432).

DNA fiber assay

Cells were treated with IdU (50 μmol/L) for 10 minutes followed by washes in warm PBS 2x, then treated with CldU (50 μmol/L) for 30 minutes. This was followed by washes in PBS 2x and then removal of cells from the plate by trypsinization. Centrifugation was carried out at 1,500 *g* (1200 rpm) for 5 min at 4°C to remove trypsin and cells were resuspended in PBS at a density of approximately 1×10^6 cells/mL. Cells were then spotted onto a clean microscope slide in a volume of 2 μL and lysed with 7 μL lysis buffer (0.5% SDS in 200 mmol/L Tris-HCl pH 7.4, 50 mmol/L EDTA) by pipetting the mixture on the slide several times and then incubating for 6 minutes at room temperature. Following lysis, slides were tilted at an angle of roughly 30° and the lysis solution was allowed to run down the slides, which were air dried and then fixed in a solution of 75% methanol/25% glacial acetic acid for 4 minutes at room temperature in a Coplin jar. Post-fixation, slides were air dried and stored overnight at 4°C. For staining, slides were first treated with 2.5 N HCl for 30 minutes at room temperature in a Coplin jar, washed 3x with PBS, and then placed in blocking solution (10% goat serum/0.1% Triton X-100 in PBS) for 1 hour at room temperature. Next, slides were incubated for 1 hour at room temperature with primary antibodies against IdU (catalog no. 347580) and CldU (catalog no. ab6326) (each at 1:100 dilution in blocking buffer) and kept in the dark. Following 3 washes with PBS, slides were incubated with secondary antibodies each at 1:350 (goat anti-mouse IgG Alexa Fluor 594 (Thermo Fisher A-11005) and goat anti-rat IgG Alex Fluor 488 (Thermo Fisher A-11006) dilution in blocking buffer and washed again 3x with PBS, air dried in the dark, and then finally mounted using 70 μL Prolong Gold mounting media (Invitrogen) with a coverslip. Slides were dried overnight and visualized on a Nikon A1 confocal microscope with a 60X objective lens. All subsequent analyses were done on NIS Elements, ImageJ, and GraphPad Prism 9.

Indirect immunofluorescence

Seventy percent confluent cell cultures prepared in 12-well plates (Mattek, catalog no. P12G-1.5–14-F) were washed 2×4°C 1x PBS (5 min/wash) and then fixed with 4% paraformaldehyde in 1x PBS for 15 minutes at room temperature. Post-fixation cells were washed 2x with ice-cold 4°C 1x PBS, permeabilized using 0.5% Triton X-100 in 1x PBS for 15 minutes at room temperature, and then incubated with 5% normal goat serum, 0.2% Triton X-100 in 1x PBS for 1 hour at room temperature to block nonspecific antibody sites. Cells were incubated with primary antibodies (1:1,000 53BP1, Cell Signaling Technology, catalog no. 4937; 1:1,000 $53BP1^{Ser25}$, Sigma, catalog no. PLA0126) overnight at 4°C followed by washing 3x with 4°C 1x PBS before incubation with the secondary antibody (anti-rabbit Alexa Fluor 594, Thermo Fisher/Invitrogen, catalog no. 11012) for 1 hour at room temperature. Following secondary antibody incubation, cells were washed 3x with PBS as described above, stained with 10 μmol/L Hoescht 33342 in 1x PBS before mounting. Image acquisition and analysis was performed as described above.

Flow cytometry

Sub-confluent cells were synchronized with aphidicolin (5 μmol/L) for 24 hours and released into fresh media. Cells were harvested at selected time points by trypsinization and spinning in a tabletop bucket centrifuge 2,000 *g* (1,500 rpm) for 5 minutes. Cells were washed and resuspended in ice cold PBS at a density of 2×10^6 cells/mL. Cells were fixed by adding cell suspension dropwise into a solution of 70% ethanol while vortexing continuously. Cells were stored at –20°C overnight and then spun down and resuspended in 500 μL propidium iodide staining solution (0.1% Triton X-100, 200 μg/mL RNAse A, 60 μmol/L propidium iodide in PBS), filtered through a nylon mesh into a polystyrene tube, and analyzed on a flow cytometer. Analysis was done with FlowJo 10.7 (FlowJo, RRID:SCR_008520) and GraphPad Prism.

PLA

The PLA was carried out using the Sigma-Aldrich Duolink Kit (catalog no. DUO92008) as described previously (23). Herein is an abridged description of the protocol. We used 12-well glass-bottomed plates and seeded cells at 1×10^5 cells per well in complete DMEM (Mediatech). Cells were washed 3x with ice cold PBS, fixed in 4% formaldehyde, and permeabilized in PBS containing 0.5% Triton X-100, and the *in situ* Red Kit Duolink (catalog no. DUO92101) was used. Blocking buffer was added at 37°C for 30 minutes, followed by primary antibodies and incubation in a humidified chamber overnight at room temperature. Wash buffer A (catalog no. DUO82049) was used to wash cells, followed by PLA Plus/Minus secondary antibody probes and incubation in a humidified chamber for 60 minutes at 37°C. Cells were then washed 2x with buffer A, followed by ligation and amplification steps (with washing in between and ligation 30 minutes at 37°C; amplification 100 minutes at 37°C). The cells were then washed 3x and mounted without coverslips. Images were taken using the Nikon A1 confocal microscope and processed with the Nikon NIS Element software, ImageJ, and Cellprofiler. The number of foci/cells were determined, and data analysis was performed in GraphPad Prism 9. PARP1 (catalog no. PLA0184, Sigma) rabbit polyclonal and PAR (catalog no. 83732, Cell Signaling Technology) rabbit polyclonal.

Immunoprecipitation

Cells were lysed in NP40 buffer (50 mmol/L Tris pH 8.0, 5 mmol/L EDTA, 150 mmol/L NaCl, 1 mmol/L dithiothreitol (DTT), 0.5% NP-40) and passed through a $21^{1/2}$ gauge needle 10x every 10 minutes at 4°C for a total of 30 minutes. Lysates were centrifuged at 15,700 *g* (13,200 rpm) for 15 minutes and supernatant transferred to a new tube. After protein quantification by the Bradford assay, 1 mg total protein was pre-cleared by adding 1 μg mouse IgG and 30 μL of protein A/G plus agarose beads (sc-2003, Santa Cruz) and rotating at 4°C for 30 minutes. Beads were spun down at 1,500 *g* (4,000 rpm) for 1 minute and the supernatant transferred to a new tube to which anti-p53 DO1-AC antibody beads (sc-126, Santa Cruz) or normal mouse IgG-AC beads (catalog no. 2343, Santa Cruz) were added. Assembled immunoprecipitation (IP) reactions were rotated at 4°C overnight. The following day, beads were spun down at 1,500 *g* (4,000 rpm) for 1 minute and washed 4x with 1 mL wash buffer (50 mmol/L Tris pH 8.0, 5 mmol/L EDTA, 150 mmol/L NaCl). After the last spin, 1x sample buffer with 50 mmol/L DTT was added on top of the beads, which were then heated at 70°C for 10 minutes, and spun down at 13,200 rpm for 1 minute. The supernatant was analyzed by SDS-PAGE.

Site-directed mutagenesis, clone validation, and transfection

We used the Nebasechanger (https://nebasechanger.neb.com) platform to design primers to introduce R273HΔ381–388 or R273HΔ347–393 changes to the plasmids pCMV-FLAG-wtp53 and pCMV-FLAG-p53R273H plasmids. For R273HΔ381–388, the primer pair was F: GGGCCTGACTCAGACTGA and R: ATGGCGGGAGGTAGACTG (the temperature for annealing was 67°C). For R273HΔ347–393, the primer pair was F: GCTGAATGAGtagTTGGAACTCAAGGATG and R: TCTCGGAACATCTCGAAG (the temperature for annealing was 57°C). Q5 Hotstart high-fidelity 2X master mix (NEB) was used for PCR reactions and product sizes were confirmed by agarose gel electrophoresis. The kinase-ligase-Dpn1 (NEB) reaction were carried out, DH5α competent cells were transformed, and specific plasmid clones were validated by sequencing (Genewiz) using a p53 Exon 8 F primer 5′ ACAGCACATGACGGAGGTTGT, and analyzed using the Benchling platform. Sequences were compared with TP53 cDNA from the GRCh38 homo sapiens reference genome. The mtp53-expressing plasmids were transfection into HCT116 p53−/− cells using Lipofectamine (Invitrogen, according to the manufacturer's instructions).

Chromatin fractionation assay

Localization of mtp53 proteins to chromosomes was assessed using a version of the chromatin fractionation assay as described (32). Herein is an abridged description of the protocol. Cells were harvested by scraping, pelleted, washed 3x with ice-cold PBS. and resuspended in 3X the pellet volume in Buffer A (10 mmol/L HEPES, 10 mmol/L KCl, 1.5 mmol/L $MgCl_2$, 300 mmol/L sucrose, 1 mmol/L DTT, 10% glycerol, 0.1 mmol/L PMSF, 1 μg/mL leupeptin, 1 μg/mL pepstatin A, and 2 μg/mL aprotinin) with 0.1% Triton X-100. Centrifugation was carried out at 1,500 *g* (4,000 rpm) for 5 minutes and the pellet containing nuclei was saved. The supernatant was spun at 15,700 *g* (13,200 rpm) for 5 minutes and saved as S1. Nuclei were washed in Buffer A + 0.15% Triton X-100 and lysed in Buffer B (3 mmol/L EDTA, 0.2 mmol/L EGTA, 1 mmol/L DTT, 0.1 mmol/L PMSF, 1 μg/mL leupeptin, 1 μg/mL pepstatin A, and 2 μg/mL aprotinin). The nuclear lysate (S2) was isolated by centrifugation for 4 minutes at 1,500 *g* (4,000 rpm) at 4°C, and chromatin was separated by washing the pellet with Buffer B followed by resuspending in Buffer B and sonication on ice to shear genomic DNA. Protein concentrations were determined using the Bradford assay (Bio-Rad). Actin and lamin were used as loading controls. Antibodies used: p53 rabbit polyclonal (catalog no. 10442–1-AP), PARP1 (catalog no. 13371–1-AP) rabbit polyclonal, actin (catalog no. sc-8432) monoclonal mouse, lamin A (catalog no. SAB420042) monoclonal mouse antibodies.

Isolation of protein on nascent DNA

The isolation of protein on nascent DNA (iPOND) assay was performed as previously described (23) with little modification. Ten 15-cm plate of cells for each cell line was cultured until each plate was 70% to 80% confluent a day before 5-ethynyl-2'-deoxyuridine (EdU) incubation. Cells were incubated with EdU diluted in complete DMEM media to a concentration of 10 μmol/L EdU for 45 minutes. Media was discarded and cells were fixed with 10 mL 0.5% formaldehyde in PBS for 20 minutes and quenched by adding 1 mL 1.25 mol/L glycine. Permeabilization of cells was done in 0.25% Triton X-100 in PBS for 30 minutes and subsequently underwent a click reaction. Click reaction was 2 mmol/L copper sulfate, 10 mmol/L biotin-azide, and 10 mmol/L sodium ascorbate added to PBS for 2 hours at room temperature with rotation. Cells were incubated in RIPA buffer on ice for 30 minutes, vortexing every 5 minutes. Additional sonication of lysate (18 on ice for 30 seconds on/off at 98% amplitude) was done after the incubation. Samples were centrifuged at 15,700 *g* (13,200 rpm) for 30 minutes at 4°C. Biotin-EdU–labeled DNA was incubated with Streptavidin–agarose beads at 4°C for 20 hours. The beads were washed 3x with RIPA buffer and proteins bound to nascent DNA were eluted by incubating in 2x SDS Laemmli sample buffer containing 0.2 mol/L DTT for 25 minutes at 95°C. Samples were run on an SDS-PAGE gel and Western blot analysis used to determine the levels of protein expression in each lane. Antibodies used: p53 rabbit polyclonal (catalog no. 10442–1-AP), PARP1 (catalog no. 13371–1-AP) rabbit polyclonal, anti-PCNA mouse monoclonal (catalog no. NBP2–80905) antibodies.

Data quantification and statistical analysis

Western blot data were quantified using ImageJ (ImageJ, RRID: SCR_003070). Statistical analyses were conducted in Excel or GraphPad Prism 9 (GraphPad Prism, RRID:SCR_002798). Results are expressed as mean + SEM. Statistical significance for hypothesis testing was performed by two-tailed Student *t* test of unknown variance and ANOVA multiple comparisons.

Results

CRISPR-cas9 mutagenesis and site directed mutagenesis

The C-terminus of wtp53, and its posttranslational modification, regulate the wtp53 transcription factor functions but how they influence mtp53 is not known (35–38). We compared alternate C-terminal versions of mtp53 R273H (**Fig. 1A**). The human TNBC cell line MDA-MB-468 expresses only mtp53 R273H and has no wtp53 (due to loss of heterozygosity). This was compared with three CRISPR-Cas9 C-terminal endogenous deletion variants. The variants included two truncated proteins, mtp53 R273HΔ381–388, and mtp53 R273HΔ347–393, as well as a frameshift mtp53 R273H*fs*387 that we previously reported reduces protein expression but does not completely eliminate mtp53 expression (**Fig. 1B**; ref. 32). We also used site directed mutagenesis to make plasmids for exogenous expression of similar C-terminal deleted mtp53 R273 proteins that could be expressed in HCT116 p53−/− cells (**Fig. 1C**).

C-terminal deletion of endogenously expressed mtp53 R273H disrupts the interaction with PARP1 and PAR

The MDA-MB-468 CRISPR-Cas9 p53 C-terminal deletion clones expressing mtp53 R273HΔ381–388 and mtp53 R273HΔ347–393 exhibit increased replication stress (32). As such, we hypothesized that the transcription-independent DNA replication function of p53 is executed by a CTD-dependent p53 function. To determine if deletion of portions of the C-terminus interrupted the ability of endogenously expressed mtp53 R273H to interact with PARP1, we used the PLA, which we previously used to report on the mtp53–PARP1 interaction (23). The PLA results demonstrated, as expected, that full-length mtp53 R273H and PARP1 are in close proximity (**Fig. 2A**, purple dots indicate foci counts per cell and per nuclei). Both the partial C-terminal deletion (R273HΔ381–388), and the complete C-terminal deletion (R273HΔ347–393), resulted in statistically significant reductions in the mtp53/PARP1 interaction per cell (**Fig. 2A** graph, R273HΔ381–388 shown by red dots, and R273HΔ347–393 shown by green dots with representative confocal microscope images also shown). In addition, we investigated whether mtp53 interacting with total PARylated proteins showed a reduced interaction when the C-terminus of mtp53 R273H was deleted. We observed a decrease in the proximity of R273HΔ347–393 C-terminally deleted mtp53 R273H with PARylated

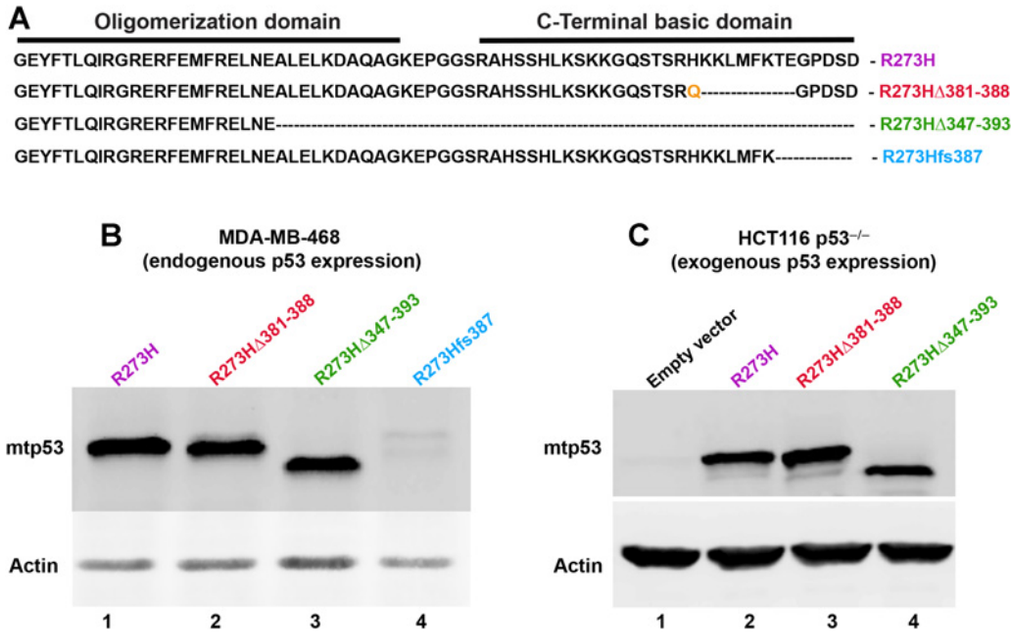

Figure 1.

CRISPR/Cas9-altered MDA-MB-468 and transfection constructs express mtp53 R273H. **A,** Schematic of mtp53 R273H protein alterations as a result of CRISPR/Cas9 alteration or site-directed mutagenesis. **B,** Western blot from whole cell lysates of MDA-MB-468 cells comparing expression levels of mtp53 R273H, mtp53 R273HΔ381–388, R273HΔ347–393, and mtp53 R273Hfs387. **C,** Western blot from whole cell lysates of HCT116 p53−/− cells transfected with plasmids encoding p53 with the same deletions. Transfection with eGFP-expressing plasmid is used as a negative control for p53 expression.

proteins but no such reduction for R273HΔ381–388 and PARylated proteins (**Fig. 2B**). This suggested that the increased portion of the C-terminus was involved in regulation of an interaction with the enzymatic product of PARP on multiple posttranslationally modified factors.

We used co-immunoprecipitation assays to assess whether the interaction of endogenously expressed C-terminal deletion mutants R273HΔ381–388 and R273HΔ347–393 resulted in less co-immunoprecipitation of PARP1. Like wtp53, mtp53 R273H co-immunoprecipitates PARP1 protein (**Fig. 2C**, lane 3; ref. 23). However, the co-immunoprecipitation experiments demonstrated that C-terminal deletion mutants R273HΔ381–388, and R273HΔ347–393, resulted in decreased interaction with PARP1 (**Fig. 2C**, lanes 6 and 9). The complete CTD deletion R273HΔ347–393, which also lacked a portion of the oligomerization domain, showed a more striking reduction in the ability to co-immunoprecipitate PARP1 (**Fig. 2C**, lane 9). Endogenously expressed mtp53 is found predominantly in the nucleus while mtp53 R273HΔ347–393 shows very low nuclear localization (32). However, when we exogenously expressed the mtp53 variants of the proteins in HCT116 p53−/− cells high levels of protein were present in the cytosol and on the chromatin (Supplementary Fig. S1A). Chromatin fractionation recapitulated our earlier finding that mtp53 R273HΔ347–393 has a lower interaction with chromatin (32) and (Supplementary Fig. S1C); but when these transfected cells were scored for mtp53-PARP PLA foci and mtp53-PAR foci we did not detect any difference for the proteins lacking the CTD (Supplementary Fig. S1B). This suggests that in addition to the CTD helping to bring the mtp53 into close proximity to PARP and PAR, the stoichiometric relationship, and the subcellular localization, of multiple cellular protein players may play a role in regulating the interactions.

Loss of the mtp53 R273H CTD and part of the oligomerization domain impair sensitivity to PARP inhibition and the response to HU-induced replication stress

The p53 protein allows cells to tolerate DNA damage in a variety of ways. One mechanism is by regulating the speed of DNA replication processivity. wtp53 slows replication speed while the site-specific DNA binding mutants R248W and R273H do not (6). Moreover, endogenous mtp53 R273H expression causes cells to be more sensitive to the PARP inhibitor talazoparib in combination with temozolomide (23, 24). We tested if MDA-MB-468 CRISPR mutated cells with a deleted CTD mtp53 had decreased sensitivity to treatment with temozolomide plus talazoparib (**Fig. 3A**). We observed no drug-induced difference in the percent reduction in mitochondrial activity for parental MDA-MB-468 expressing full length mtp53 R273H in comparison with the cells expressing mtp53 R273HΔ381–388, but the cells expressing mtp53 R273HΔ347–393 were less sensitive to temozolomide plus talazoparib (**Fig. 3A**). Cells expressing mtp53 R273H with the CTD deleted proliferate more slowly than the parental MDA-MB-468 cells while also not having a substantially different cell-cycle profile (32). Therefore, we compared the viability of the three cell lines to determine if perhaps the cells had a lower proportion able to survive. We compared the ability of the cells to take up propidium iodide, as well as the basal MTT values. We found that there was no statistically significant difference in the baseline mitochondrial activity but that the cells expressing mtp53 R273HΔ347–393 had the highest propidium iodide uptake, which was an indication that they might be less viable by an unknown mechanism (**Fig. 3B**). Therefore, the reduced sensitivity to temozolomide plus talazoparib of cells expressing mtp53 R273HΔ347–393 may be the result of an already compromised state of low cell proliferation and viability.

Chromosomal DNA replication is modified by mtp53 R273H and mtp53 R248W in such a way that their expression inhibits

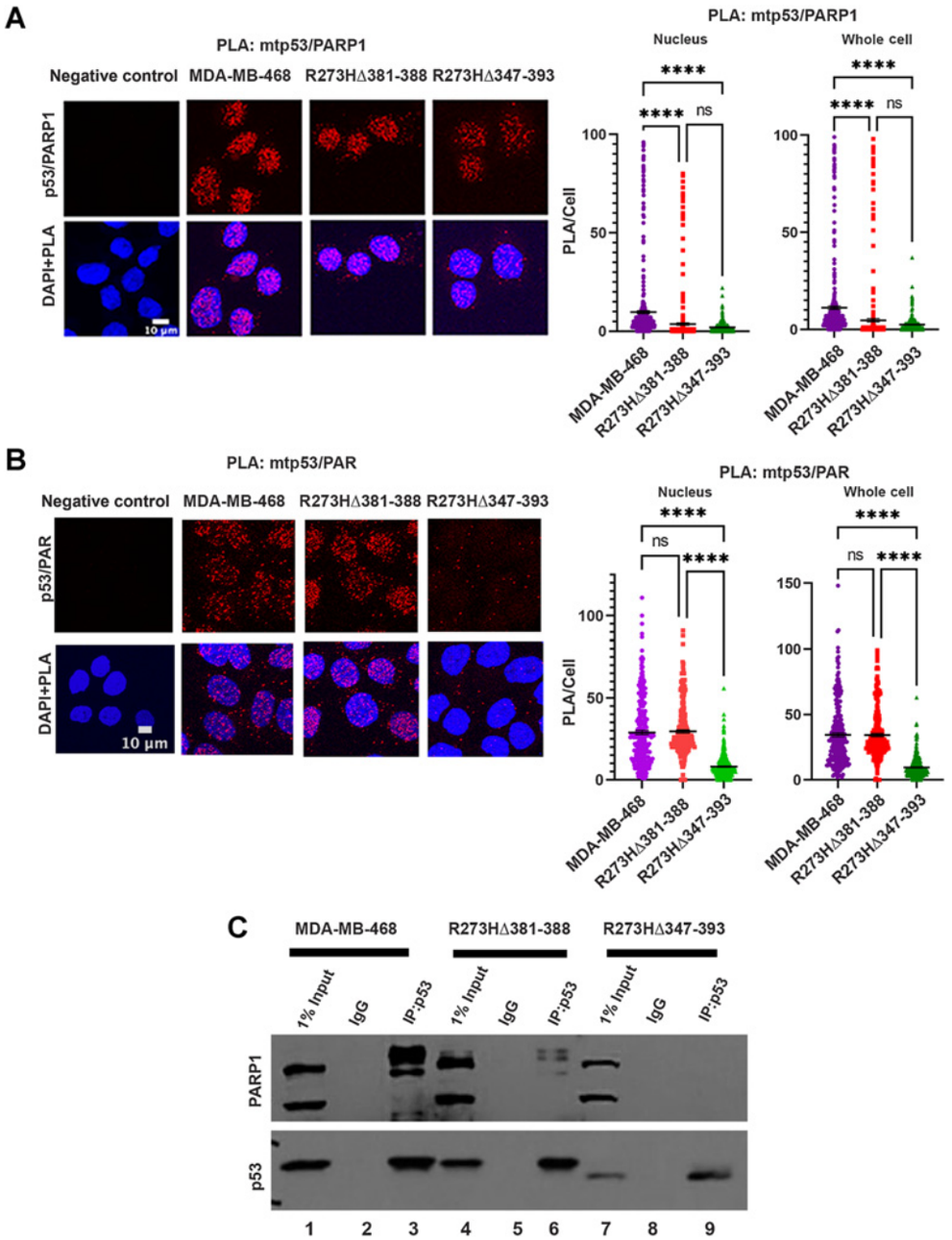

Figure 2.

Loss of the CTD of R273H mtp53 decreases mtp53-PARP1 and mtp53-PAR interactions. **A,** Analysis of p53/PARP1 complexes by *in situ* PLA in MDA-MB-468, R273HΔ381–388, and R273HΔ347–393 cells. Fluorescent foci per cell were counted by Cellprofiler software and depicted by a scatter plot using GraphPad Prism 9. The data represent a scatter plot with $n = 3$. An ordinary one-way ANOVA was used to determine the statistical significance of the data. The following format was used to assign significance based on P value.****, $P \leq 0.0001$; ns, nonsignificant. Representative confocal microscope images of p53/PARP1 foci/complexes (red) by *in situ* PLA in MDA-MB-468, R273HΔ381–388, and R273HΔ347–393 cells. DNA was counterstained with DAPI (blue). The z-stack maximum intensity projection images are shown. Three independent experiments were performed. (Scale bar = 10 μm). The negative control scoring for both panels **A** and **B** was single antibody probing for p53 followed by all other PLA steps. **B,** Analysis of p53/PAR complexes by *in situ* PLA in MDA-MB-468, R273HΔ381–388 and R273HΔ347–393 cells. Fluorescent foci per cell were counted by Cellprofiler software and depicted by a scatter plot using GraphPad Prism 9. The data represent a scatter plot with $n = 3$. An ordinary one-way ANOVA was used to determine the statistical significance of the data. The following format was used to assign significance based on P value. ****, $P \leq 0.0001$; ns, nonsignificant. Representative confocal microscope images of p53/PAR foci/complexes (red) by *in situ* PLA in MDA-MB-468, R273HΔ381–388, and R273HΔ347–393 cells. DNA was counterstained with DAPI (blue). The z-stack maximum intensity projection images are shown. Three independent experiments were performed. (Scale bar = 10 μm). **C,** Pellets from MDA-MB-468, R273HΔ381–388 and R273HΔ347–393 cells were lysed in NP-40 buffer and lysate used for co-immunoprecipitation assay. Samples were run on an SDS-PAGE gel and Western blot analysis performed with p53 and PARP1 antibodies. Lanes 1, 4, and 7 represent the input lanes, lanes 2, 5, and 8 represent the negative control IgG lanes and lanes 3, 6, and 9 represent the p53: IP lanes. Image is a representation of 3 independent biological replicates.

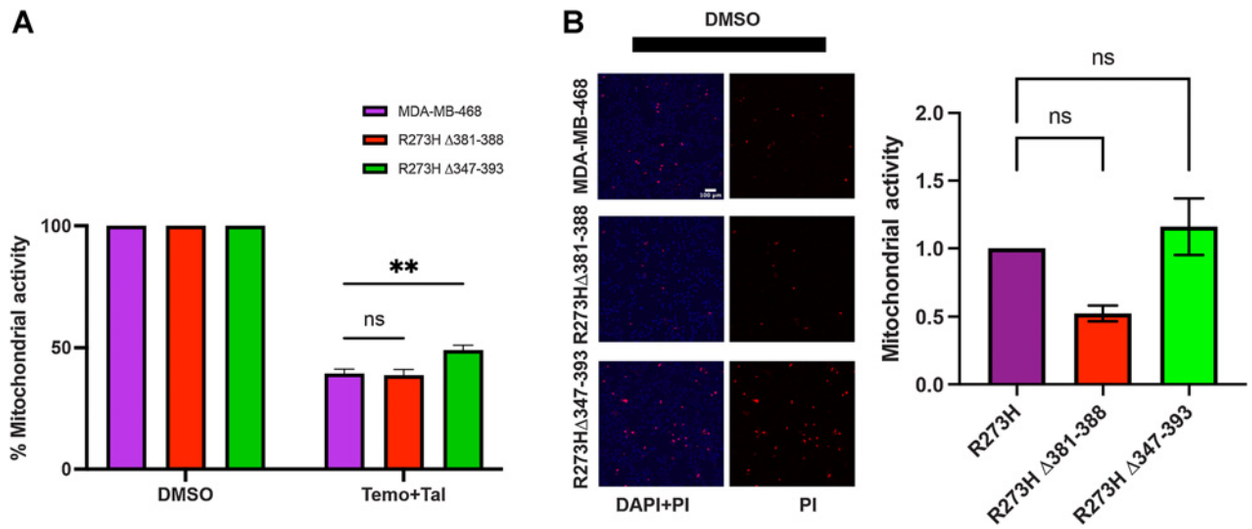

Figure 3.

MDA-MB-468 cell expressing R273HΔ347–393 are less sensitive to temozolomide plus talazoparib. **A,** MTT assay was used to determine the cell viability of mtp53 R273H expressing MDA-MB-468 compared with R273HΔ381–388 or R273HΔ347–393 in response to a 24-hour combination treatment with Temo (1 mmol/L) and Tal (10 μmol/L) or a DMSO vehicle control. The data is a representation of three independent biological replicate. An ordinary one-way ANOVA with multiple comparison was used to determine the statistical significance of the data. The following format was used to assign significance based on *P* value. **, $P \leq 0.001$; ns, nonsignificant $P > 0.0$. **B,** Confocal maximum projection of live-cell imaging of mtp53 R273H expressing MDA-MB-468 compared with R273HΔ381–388 or R273HΔ347–393 MDA-468 cells in response to a 24-hour combination treatment with Temo (1 mmol/L) and Tal (10 μmol/L) with DMSO as the vehicle control. DNA was counterstained with DAPI (blue). Red fluorescence was propidium iodide staining. MTT assay was used to determine the cell viability of mtp53 R273H expressing MDA-MB-468 compared with R273HΔ381–388 or R273HΔ347–393 cells. The data is a representation of three independent biological replicate. An ordinary one-way ANOVA with multiple comparison was used to determine the statistical significance of the data. The following format was used to assign significance based on *P* value. ns, nonsignificant $P > 0.0$.

HU-mediated replication stress by promoting the interaction of TopBP1 with Treslin (39). PARP is also involved in protecting replication forks, and inhibition of PARP protein increases replication processivity which results in cell death by mitotic catastrophe through increased Okazaki ssDNA gaps (21, 40). We used DNA fiber analysis to test if the alteration of the C-terminus of mtp53 R273H in MDA-MB-468 cells resulted in different fork speeds, and/or differential responses to replication stress induction by HU treatment (**Fig. 4**). All cell lines treated with HU demonstrated statistically significant reduced replication speeds (compare **Fig. 4A**–**D**, left). The origin firing of these cell lines did not show a statistically significant change in the presence of HU (see Supplementary Fig. S2). Replication stress takes many forms including increasing replication fork asymmetry resulting from fork stalling and uncoupling; such asymmetry can be detected by DNA fiber analysis (41). We examined the HU-induced fork asymmetry in the cell lines (**Fig. 4A**–**D**, see panels). When cells were treated with HU, the cells expressing mtp53 R273HΔ347–393 did not experience a statistically significant increase in fork asymmetry (**Fig. 4C**), while full-length, mtp53 R273HΔ381–388, and R273Hfs387 all responded to HU-treatment with increased fork asymmetry (**Fig. 4A**, **B**, **D**). This suggests the mtp53 R273H, the mtp53 R273HΔ381–388, and that the low level of mtp53 expressed in the cells with mtp53 R273Hfs387 can drive DNA synthesis even in the presence of HU whereas mtp53 R273HΔ347–393, lacking the CTD, is deficient in this activity.

C-terminal deletion of mtp53 R273H reduces p53 on replicating DNA and decreases the ability of cells to proceed through the G_2–M checkpoint

We assessed if removal of the mtp53 R273H C-terminus influenced the interaction of mtp53 or PARP with replicating DNA, or if such deletions influenced the progression of MDA-MB-468 cells through the cell cycle. We used immunoprecipitation of nascent DNA to evaluate the interaction of mtp53 proteins, PARP1, and PCNA on replicating DNA in the MDA-MB-468 cells with either mtp53 R273H, mtp53 R273HΔ381–388, or mtp53 R273HΔ347–393 (**Fig. 5A**). We observed that the overall interactions of PARP1 and PCNA with replicating DNA were not reduced by removal of the mtp53 C-terminus (**Fig. 5A**, see PARP1 and PCNA). In fact, they appeared to increase. This may be because they are needed to assist with the increased replication stress. As expected, there was very low mtp53 R273HΔ347–393 on nascent DNA and reduced mtp53 R273HΔ381–388 on nascent DNA (**Fig. 5A**). Previously, we evaluated these cells for S-phase cell-cycle progression by flow cytometry and observed small delays in the progression of cells containing R273HΔ381–388 and R273HΔ347–393 mutations and a large delay in cells containing the R273Hfs387 mutation (32). Here, we evaluated the progression of the C-terminal deletion mutants via flow cytometry following synchronization with aphidicolin for 24 hours. The low asymmetry observed for mtp53 R273HΔ347–393 HU-treated cells, did not translate into any difference observed for the release from aphidicolin cell-cycle block (even though their general proliferation and cell viability was reduced). We observed that cells harboring the R273HΔ381–388 mutant following synchronization with aphidicolin started with more cells in G_2–M as compared with cells expressing either full length R273H or R273HΔ347–393 (**Fig. 5B**–**D**). After a 20-hour release from aphidicolin we observed that cells expressing the mtp53 R273HΔ381–388 recovered and all the profiles looked similar. These data indicated that MDA-MB-468 cells expressing mtp53 R273HΔ381–388 had a delayed progression through the cell cycle. We tested if this delay was in G_2–M of the cell cycle by blocking the cells with nocodazole and then examining cell cycle progression after release (**Fig. 5E**–**G**). The cells showing the slowest recovery were the MDA-MB-468 cells expressing

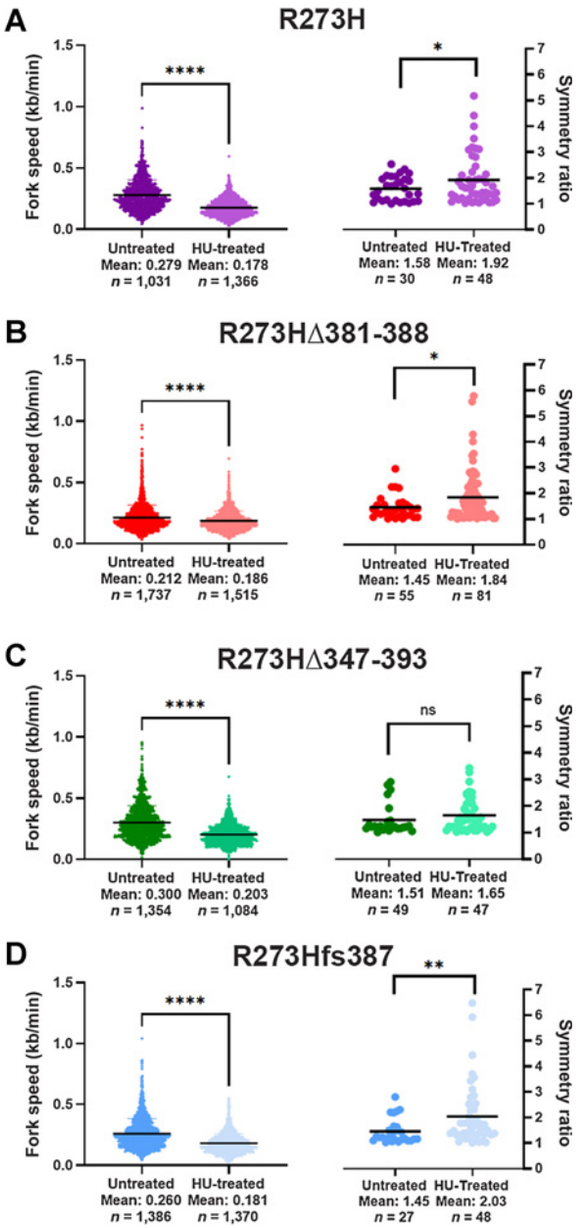

Figure 4.

The mtp53 R273H CTD alters DNA replication dynamics under HU treatment. (**A–D**, left) DNA fiber assay comparing fork speed in MDA-MB-468, R273HΔ381–388, R273HΔ347–393, and R273Hfs387 cells. Fork speed was determined through measuring the CldU length of double labeled DNA fibers. (**A–D**, right) Asymmetry ratio was determined through measuring both arms of newly fired origins and dividing the length of the long arm over the short arm of the same origin. Three independent biological replicates were performed. Pairwise comparisons were made using ANOVA. *, $P < 0.05$; **, $P < 0.01$; ****, $P < 0.0001$; ns, nonsignificant $P > 0.0$.

the mtp53 R273HΔ381–388, which was also indicated by their sustained increased level of RRM2 protein (**Fig. 5E–G**). The protein RRM2 is reduced by proteolytic digestion as cells progress into G1 from G_2–M (42).

Cell proliferation can be blocked by replication stress caused by incomplete DNA replication. An indicator of such incomplete replication due to increase ssDNA gaps from unprocessed Okazaki fragments is an increase in 53BP1 foci (21). As such we compared the phosphorylated 53BP1 foci per cell for the different cell lines (**Fig. 6**). We predicted that as compared with the fast proliferation of MDA-MB-468 cells, the slow proliferating cell lines expressing mtp53 R273HΔ347–393 and R273HΔ381–388 would be accompanied by increased phosphorylated 53BP1 foci. We observed a statistically significant increase in the 53BP1 foci when we compared the MDA-MB-468 cells expressing full-length p53 to both the cells expressing mtp53 R273HΔ347–393 and mtp53 R273HΔ381–388 (**Fig. 6**, representative image and quantitative graph). There was no statistically significant difference between cells expression mtp53 R273HΔ381–388 or mtp53 R273HΔ347–393; as such the pronounced G_2–M checkpoint for the cells expressing mtp53 R273HΔ381–388 could be because they contain more C-terminal amino acid sequence that allows for mtp53 tetramerization and an interaction with MDM2 (43). MDM2 binds to, and regulates PARP1 (44). Monomeric mtp53 R273H lacking Δ347–393 has presumably lost C-terminal interactions with MDM2 that are different in cells expressing mtp53 R273HΔ381–388.

Discussion

The CTD of mtp53, like wtp53, regulates the interaction with PARP1

The CTD of p53 has been shown to have many functions that regulate wtp53 activity; this includes interactions with multiple proteins, and sites for posttranslational modifications (**Fig. 7A**; ref. 1). Changes to the C-terminus of p53 in mouse models interfere with development and result in lethality (36–38). The CTD of wtp53 is a central hub for the non-covalent interaction with PARylated PARP1 and PARylation posttranslational modification (17). The CTD of both wtp53 and synthetically designed DNA binding mutants interact strongly with poly ADP ribose chains (45). We found that MDA-MB-468 cells endogenously expressing mtp53 R273HΔ347–393 had a decreased mtp53 interaction with PARP1 and other PARylated proteins in cell nuclei while mtp53 R273HΔ381–388 only showed a decreased interaction with PARP1 (**Fig. 2**). When the different variant mtp53 R273H were exogenously expressed in HCT 116 p53−/− cells, extremely high mtp53 was seen in both the cytosol and nucleus. The PLA-foci could not be distinguished for nuclear versus cytoplasm per cell and mtp53 PARP and PARylated protein interactions were not reduced by the CTD deletions (Supplementary Fig. S1). We predict that this is due to abnormally high mtp53 expression that causes high proximity to multiple factors in the cytosol and the nucleus. DNA (and poly-ADP-ribose interactions) may be assisting in the close proximity interaction, as the mtp53 interactions were more robustly seen using the PLA assay than co-immunoprecipitation, and were altered by transient transfection and exogenous expression of the mtp53 variant proteins.

Potential reasons for connections between mtp53 and PARP and PAR

The non-covalent interaction of mtp53 R273H with PARP1 and PAR may serve multiple regulatory functions. First, this interaction may serve to help stabilize mtp53 R273H in cells. Second, mtp53–PARP interaction may assist in regulation of chromatin organization, as PARylation of chromatin factors is known to regulate chromatin remodeling (46, 47). PARP1 can enzymatically PARylate many proteins that have C-terminally disordered regions like p53 (17, 45). One interpretation for why mtp53 R273H may have a strong connection to

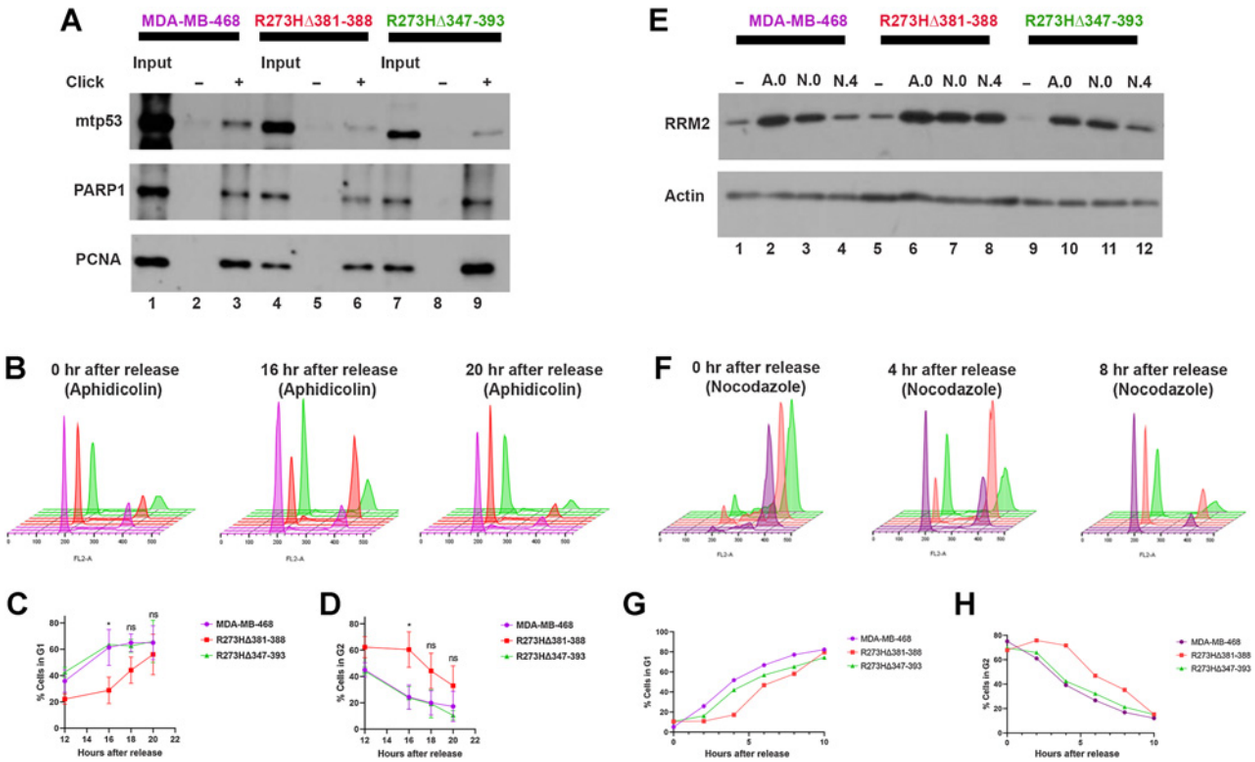

Figure 5.

mtp53 R273H localizes to replicating DNA and changes cell-cycle dynamics. **A,** iPOND experiment comparing MDA-MB-468, R273HΔ381–388, and R273HΔ347–393 cells. PCNA is used as a positive control for pulldown of nascent DNA. **B,** Flow cytometry comparing MDA-MB-468, R273HΔ381–388, and R273HΔ347–393 cells. Cells were treated with aphidicolin for 24-hour and released into fresh media. Measurements were taken from 0 to 20 hours as indicated. Three independent biological replicates were performed but data is shown from one independent biological replicate. **C** and **D,** Summary analysis of flow cytometry data over time. Three independent biological replicates were performed. Statistical comparisons were made using a one-tailed Student *t* test. *, $P < 0.05$. **E,** Western blot comparing protein levels of cell-cycle marker RRM2 between MDA-MB-468, R273HΔ381–388, and R273HΔ347–393 cells. This experiment follows asynchronous cells (-), cells synchronized with aphidicolin (A.0), nocodazole (N.0), or a nocodazole synchronization and release for 4 hours (N.4). Actin is used as a loading control. **F,** Flow cytometry comparing MDA-MB-468, R273HΔ381–388, and R273HΔ347–393 cells. Cells were treated with aphidicolin for 24 hours and released into fresh media followed by treatment with nocodazole. Cells were then released into fresh media and measurements were taken from 0 to 10 hours as indicated. Data for MDA-MB468 and R273HΔ381–388 is representative of three independent biological replicates while data from R273HΔ347–393 represents one biological replicate. **G–H,** Summary analysis of flow cytometry data over time.

PARylated PARP1 is because this hot-spot mtp53 has lost site-specific DNA binding activity. The freedom that mtp53 has from binding site-specifically to DNA, and also potentially from binding to 53BP1, may allow mtp53 to more strongly interact non-covalently with PARylated PARP1 (45, 48).

The mtp53 R273 protein may use the CTD to interact with PARylated PARP on nuclear DNA and stabilize interactions to better carryout Okazaki fragment processing (**Fig. 7B**). The observed increase in 53BP1 foci in cells lacking portions of the mtp53 R273H CTD, and the reduction in cell proliferation, provide data to suggest a model (**Figs. 6** and **7**; ref. 21). The increased stability of mtp53 as compared with wtp53 would provide a setting in which a normally limited DNA repair mechanism for wtp53 takes on a gained function that provokes genomic instability in cancer cells. Interestingly, mtp53 does not directly interact with 53BP1 (49). Therefore the influence of wtp53 versus mtp53 interacting with PARP at Okazaki fragment processing foci may function very differently. We see PARP1 binding to replicating DNA in the presence, or absence, of the mtp53 R273H CTD (**Fig. 5A**). PARP1 associates with the lagging strand and assists in Okazaki fragment processing (19, 21), but the interaction of the CTD of mtp53 with the PARP1 has never been shown to contribute this DNA replication safeguard. The mtp53–PARP1 axis may coordinate a bridge between mtp53 and other mtp53 binding partners like MCM2–7 and topoisomerase 1 (50). Nuclear PARPs are critical for maintaining genome integrity during DNA replication, but exactly what they do in cancer cells undergoing increased genomic instability requires further study (46). We see that PARylated PARP1 in MDA-MB-468 breast cancer cells interacts with the CTD of mtp53 R273H, and this may allow for the coordination of replication proteins needed to respond to replication stress (**Fig. 7**). Future experiments to test Okazaki fragment processing, should include DNA-combing with and without S1 nuclease in cells expressing mtp53 with, and without, CTD mutations.

We observed that cells expressing the mtp53 CTD deletion R273HΔ381–388 had a delay in progressing through G_2–M cells after aphidicolin synchronization (**Fig. 5**). Resolving why the mtp53 R273HΔ381–388 expressing cells show this phenotype while the mtp53 R273HΔ347–393 cells do not requires future experiments to explore the interaction with additional proteins (that may or may not be PARylated proteins). It is possible that because mtp53 R273HΔ381–388 retains association with other PARylated proteins, but has lost a critical PARP1 association, it then provokes a G_2–M checkpoint.

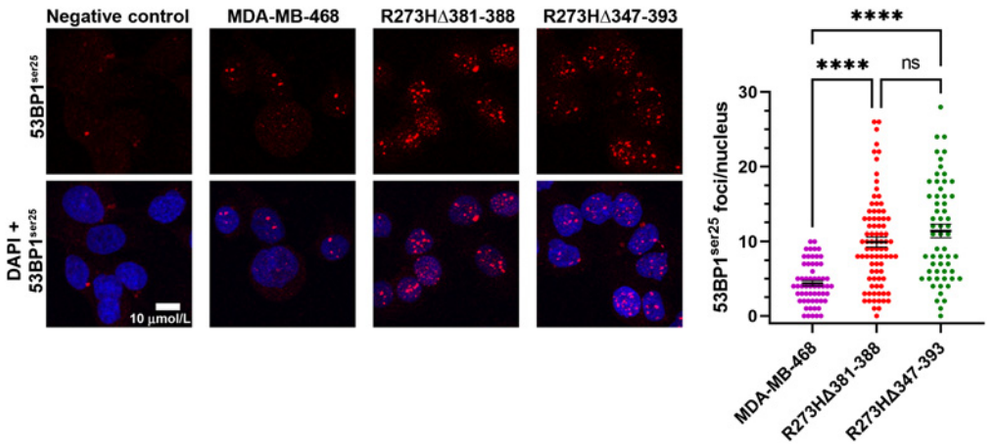

Figure 6.

Deletion of mtp53 R273H CTD increases 53BP1 foci. 53BP1^{ser25} foci abundance within MDA-MB-468, R273HΔ381–388 and R273HΔ347–393 cells was examined as described in the Materials and Methods by indirect immunofluorescence using Alexa Fluor 594-linked secondary antibody to detection of antibody-53BP1^{ser25} complexes (red, top); overlay with Hoescht 33342-stained DNA (blue) was performed to assess nuclear localization (bottom). Foci abundance per cell was determined using Cell Profiler software and represented in a scatter plot using GraphPad Prism 9. A one-way ANOVA was performed to evaluate statistical significance between the cell lines with *P* value. ****, $P \leq 0.0001$.

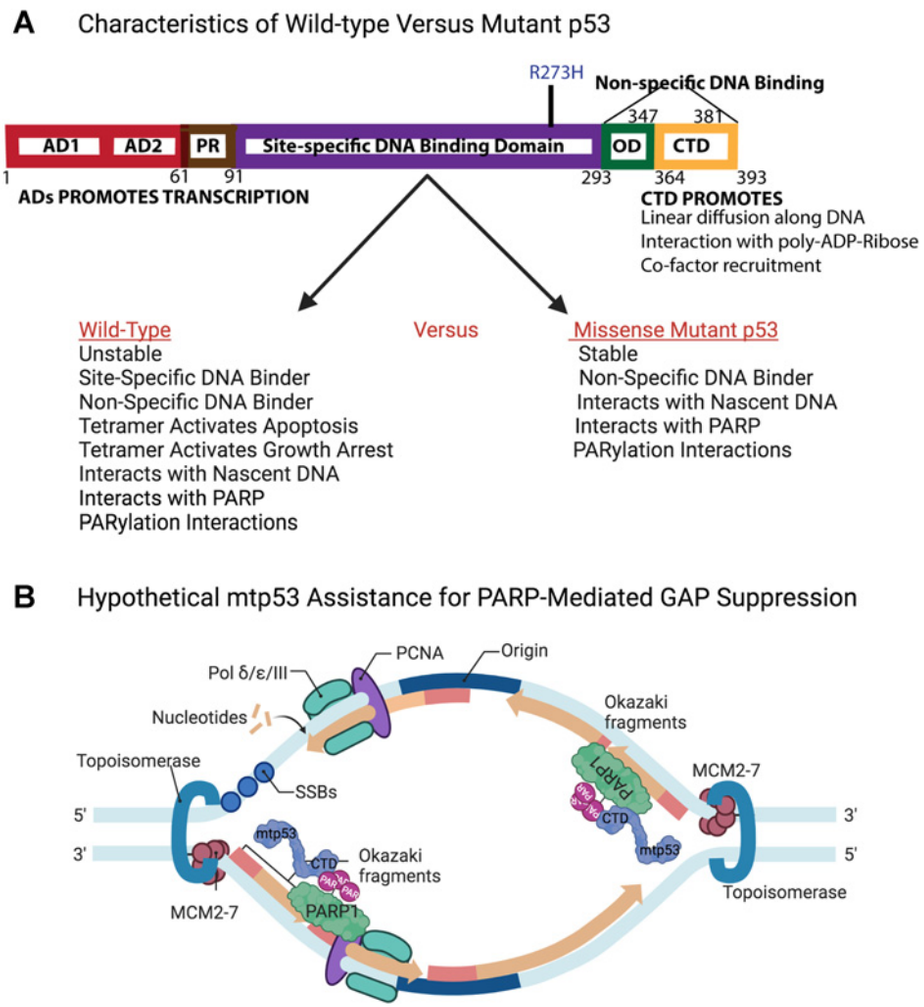

Figure 7.

Model for mtp53 CTD cross-talk with PARP1 replicating DNA. **A,** We provide a review of some differences between wtp53 and mtp53 R273H. **B,** Speculative model for our data, which indicates that the mtp53 R273H CTD interacts with replicating DNA, PARP1, and PAR. We predict in that this interaction occurs on the lagging strand of DNA replication forks and assists in the efficient resolution of DNA replication stress in cancer cells by improving Okazaki fragment processing. This model was created using Biorender.

Future studies needed to determine if PARP1 activity is regulated by mtp53 and how mtp53 posttranslational modification regulates PARP1 interactions

The C-terminus of mtp53 R273H may regulate both the PARylation of mtp53, and the interaction with PARP1, in such a way that PARP1 enzymatic activity and substrate selection are altered. We propose that in cells expressing mtp53 R273HΔ347–393, the leading strand is uncoupled from the lagging strand and allows for increased processivity as well as less replication fork asymmetry (**Fig. 7**). In cells with mtp53 R273HΔ381–388, the altered mtp53 may have interactions with some PARylated PARP1, and some unPARylated PARP1. While we do not have direct evidence for an altered interaction between mtp53 R273HΔ381–388 and PARP1, it remains a possibility that this mtp53 isoform had distinct protein–protein interactions that will need to be identified. The different outcomes on the G_2–M cell-cycle progression for cells expressing mtp53 R273HΔ381–388 suggests that a cross-talk with multiple mtp53 associated proteins occurs to elicit a G_2 checkpoint for this version of mtp53 that maintains interaction with PARylated proteins that are not PARP.

Replication fork speed is increased under conditions of PARP1 inhibition, or depletion, and this causes more cell death because Okazaki fragment processing is reduced (40). If mtp53 helps PARylated PARP improve Okazaki fragment processing through CTD–PARP interactions then the interactions with additional proteins may signal for checkpoints when processing is not complete. The possibility that mtp53 R273HΔ347–393 lacks a PARP1-mediated damage sensing mechanism is supported by the absence of a statistically significant change in replication fork asymmetry between untreated and HU-treated conditions and temozolomide plus talazoparib (**Fig. 4**). While deletion of amino acids 347–393 decreased the sensitivity of cells to HU and temozolomide plus talazoparib, the deletion of mtp53 R273H amino acids 381–388 delayed G_2–M progression. The model shown in **Fig. 7** displays our hypothetical view of how the mtp53 CTD might participate in GOF aberrant repair by interacting with chromatin-bound PARP1 and supporting resolution of unligated Okazaki fragments.

Targeting PARP1 inhibition may be a valuable strategy for breast cancers that express mtp53 and PARP1 biomarkers

PARP1 inhibitors with varying activities are prescribed for people with breast cancers that have BRCA1 mutations, but not for cancers that have p53 mutations (29). Further understanding the relationship that mtp53 plays in the response of cancers to single, or combination, treatments with the new array of PARP1 inhibitors will extend the demographics for precision medicine patients. The interplay between p53 and PARP1 is dynamic, and creates a central hub for evaluating cellular regulation pathways (17, 51, 52). Immunohistochemistry is used to detect high expression of mtp53 and PARP proteins, which are both often found in breast cancers (23). We have seen that high expression of mtp53 R273H sensitizes breast cancer cells to killing by the combination treatment of the PARP1 inhibitor talazoparib in combination with the chemotherapeutic agent temozolomide (23, 24). Future goals should be to determine the role of different missense mtp53, posttranslationally modified mtp53, and complete loss of expression of p53, as biomarkers for sensitivity to PARP1 inhibitor combination treatments. Patients with TNBC have the unmet need of positive biomarkers that can be used to determine personalized therapies. The interaction of the CTD of mtp53 with PARP1 suggests that adding the co-expression of these two biomarkers to the list may have major benefits.

Authors' Disclosures

V. Chavez reports grants from NIH; and grants from The Breast Cancer Research Foundation during the conduct of the study. S. Maimos reports grants from NIH; and grants from The Breast Cancer Research Foundation during the conduct of the study. Z. Syed reports grants from NIH; and grants from The Breast Cancer Research Foundation during the conduct of the study. S. Jiang reports grants from NIH; and grants from The Breast Cancer Research Foundation during the conduct of the study. V. Ellison reports grants from NIH; and grants from The Breast Cancer Research Foundation during the conduct of the study. J. Bargonetti reports grants from NIH; and grants from The Breast Cancer Research Foundation during the conduct of the study. No disclosures were reported by the other authors.

Disclaimer

Its contents are solely the responsibility of the authors and do not necessarily represent the official views of the NCI/NIH.

Authors' Contributions

D. Lundine: Conceptualization, formal analysis, funding acquisition, validation, investigation, visualization, writing–original draft, project administration, writing–review and editing. **G.K. Annor:** Conceptualization, formal analysis, funding acquisition, validation, investigation, writing–original draft, project administration, writing–review and editing. **V. Chavez:** Investigation, writing–review and editing. **S. Maimos:** Formal analysis, validation, investigation. **Z. Syed:** Formal analysis. **S. Jiang:** Investigation. **V. Ellison:** Supervision, investigation, methodology, writing–review and editing. **J. Bargonetti:** Conceptualization, resources, formal analysis, supervision, funding acquisition, validation, methodology, writing–original draft, project administration, writing–review and editing.

Acknowledgments

This work was supported by The Breast Cancer Research Foundation BCRF-20–011 and BCRF-21–011 to J. Bargonetti, and by NIH grants R01 R01CA239603 to J. Bargonetti. This work was also partially supported by the TUFCCC/HC Regional Comprehensive Cancer Health Disparity Partnership from the NIH to D. Lundine and G.K. Annor, U54 CA221704 and NIH-RISE 5R25GM060665–22 funds to V. Chavez. We thank Dr. Gu Xiao for providing valuable assistance preparing figures and Drs. Maria Jasin and Pei Xin Lim for the detailed DNA fiber assay protocol.

The publication costs of this article were defrayed in part by the payment of publication fees. Therefore, and solely to indicate this fact, this article is hereby marked "advertisement" in accordance with 18 USC section 1734.

Note

Supplementary data for this article are available at Molecular Cancer Research Online (http://mcr.aacrjournals.org/).

Received February 16, 2022; revised August 2, 2022; accepted September 2, 2022; published first September 8, 2022.

References

1. Pfister NT, Prives C. Transcriptional regulation by wild-type and cancer-related mutant forms of p53. Cold Spring Harb Perspect Med 2017;7:a026054.
2. The Cancer Genome Atlas. Comprehensive molecular portraits of human breast tumors. Nature 2012;490:61–70.
3. Bargonetti J, Prives C. Gain-of-function mutant p53: history and speculation. J Mol Cell Biol 2019;11:605–9.
4. Gottifredi V, Wiesmuller L. The tip of an iceberg: replication-associated functions of the tumor suppressor p53. Cancers 2018;10:250.

5. Ho T, Tan BX, Lane D. How the other half lives: what p53 does when it is not being a transcription factor. Int J Mol Sci 2019;21:13.
6. Biber S, Pospiech H, Gottifredi V, Wiesmuller L. Multiple biochemical properties of the p53 molecule contribute to activation of polymerase iota-dependent DNA damage tolerance. Nucleic Acids Res 2020;48:12188–203.
7. Roy S, Tomaszowski KH, Luzwick JW, Park S, Li J, Murphy M, et al. p53 orchestrates DNA replication restart homeostasis by suppressing mutagenic RAD52 and POLθ pathways. Elife 2018;7:e31723.
8. Klusmann I, Rodewald S, Muller L, Friedrich M, Wienken M, Li Y, et al. p53 activity results in DNA replication fork processivity. Cell Rep 2016;17:1845–57.
9. Janz C, Wiesmuller L. Wild-type p53 inhibits replication-associated homologous recombination. Oncogene 2002;21:5929–33.
10. Hampp S, Kiessling T, Buechle K, Mansilla SF, Thomale J, Rall M, et al. DNA damage tolerance pathway involving DNA polymerase iota and the tumor suppressor p53 regulates DNA replication fork progression. Proc Natl Acad Sci USA 2016;113:E4311–9.
11. Wang YH, Ho TLF, Hariharan A, Goh HC, Wong YL, Verkaik NS, et al. Rapid recruitment of p53 to DNA damage sites directs DNA repair choice and integrity. Proc Natl Acad Sci USA 2022;119:e2113233119.
12. Hoffman S, Martin D, Melendez A, Bargonetti J. C. elegans CEP-1/p53 and BEC-1 are involved in DNA repair. PLoS One 2014;9:e88828.
13. Notterman D, Young S, Wainger B, Levine AJ. Prevention of mammalian DNA reduplication, following the release from the mitotic spindle checkpoint, requires p53 protein, but not p53-mediated transcriptional activity. Oncogene 1998;17:2743–51.
14. Tafvizi A, Huang F, Fersht AR, Mirny LA, van Oijen AM. A single-molecule characterization of p53 search on DNA. Proc Natl Acad Sci USA 2011;108:563–8.
15. Wesierska-Gadek J, Wojciechowski J, Schmid G. Phosphorylation regulates the interaction and complex formation between wt p53 protein and PARP-1. J Cell Biochem 2003;89:1260–84.
16. Wesierska-Gadek J, Wojciechowski J, Schmid G. Central and carboxy-terminal regions of human p53 protein are essential for interaction and complex formation with PARP-1. J Cell Biochem 2003;89:220–32.
17. Fischbach A, Kruger A, Hampp S, Assmann G, Rank L, Hufnagel M, et al. The C-terminal domain of p53 orchestrates the interplay between non-covalent and covalent poly(ADP-ribosyl)ation of p53 by PARP1. Nucleic Acids Res 2018;46:804–22.
18. Rudolph J, Muthurajan UM, Palacio M, Mahadevan J, Roberts G, Erbse AH, et al. The BRCT domain of PARP1 binds intact DNA and mediates intrastrand transfer. Mol Cell 2021;81:4994–5006.
19. Hanzlikova H, Kalasova I, Demin AA, Pennicott LE, Cihlarova Z, Caldecott KW. The importance of Poly(ADP-Ribose) polymerase as a sensor of unligated okazaki fragments during DNA replication. Mol Cell 2018;71:319–31.
20. Hanzlikova H, Caldecott KW. Perspectives on PARPs in S phase. Trends Genet 2019;35:412–22.
21. Cong K, Peng M, Kousholt AN, Lee WTC, Lee S, Nayak S, et al. Replication gaps are a key determinant of PARP inhibitor synthetic lethality with BRCA deficiency. Mol Cell 2021;81:3128–44.
22. Caldecott KW. DNA single-strand break repair and human genetic disease. Trends Cell Biol 2022;32:733–45.
23. Xiao G, Lundine D, Annor GK, Canar J, Ellison V, Polotskaia A, et al. Gain-of-function mutant p53 R273H interacts with replicating DNA and PARP1 in breast cancer. Cancer Res 2020;80:394–405.
24. Qiu WG, Polotskaia A, Xiao G, Di L, Zhao Y, Hu W, et al. Identification, validation, and targeting of the mutant p53-PARP-MCM chromatin axis in triple-negative breast cancer. NPJ Breast Cancer 2017;3:1.
25. Polotskaia A, Xiao G, Reynoso K, Martin C, Qiu WG, Hendrickson RC, et al. Proteome-wide analysis of mutant p53 targets in breast cancer identifies new levels of gain-of-function that influence PARP, PCNA, and MCM4. Proc Natl Acad Sci USA 2015;112:E1220–9.
26. Shtraizent N, Matsui H, Polotskaia A, Bargonetti J. Hot-spot mutation in TP53 (R248Q) causes oncogenic gain-of-function phenotypes in a breast cancer cell line derived from an African American patient. Int J Environ Res Public Health 2016;13:ijerph13010022.
27. Hobbs EA, Litton JK, Yap TA. Development of the PARP inhibitor talazoparib for the treatment of advanced BRCA1 and BRCA2 mutated breast cancer. Expert Opin Pharmacother 2021:1–13.
28. Chen Z, Wang X, Li X, Zhou Y, Chen K. Deep exploration of PARP inhibitors in breast cancer: monotherapy and combination therapy. J Int Med Res 2021;49:300060521991019.
29. Ashworth A, Lord CJ. Synthetic lethal therapies for cancer: What's next after PARP inhibitors? Nat Rev Clin Oncol 2018;15:564–76.
30. Wilson T, Pirovano G, Xiao G, Samuels Z, Roberts S, Viray T, et al. PARP-targeted auger therapy in p53 mutant colon cancer xenograft mouse models. Mol Pharm 2021;18:3418–28.
31. Annor GK, Elshabassy N, Lundine D, Conde DG, Xiao G, Ellison V, et al. Oligomerization of mutant p53 R273H is not required for gain-of-function chromatin associated activities. Front Cell Dev Biol 2021;9:772315.
32. Ellison V, Annor GK, Freedman C, Xiao G, Lundine D, Freulich E, et al. Frame-shift mediated reduction of gain-of-function p53 R273H and deletion of the R273H C-terminus in breast cancer cells result in replication-stress sensitivity. Oncotarget 2021;12:1128–46.
33. Bunz F, Dutriaux A, Lengauer C, Waldman T, Zhou S, Brown JP, et al. Requirement for p53 and p21 to sustain G2 arrest after DNA damage. Science 1998;282:1497–501.
34. Bunz F, Hwang PM, Torrance C, Waldman T, Zhang Y, Dillehay L, et al. Disruption of p53 in human cancer cells alters the responses to therapeutic agents. J Clin Invest 1999;104:263–9.
35. Laptenko O, Tong DR, Manfredi J, Prives C. The tail that wags the dog: how the disordered C-terminal domain controls the transcriptional activities of the p53 tumor-suppressor protein. Trends Biochem Sci 2016;41:1022–34.
36. Kon N, Churchill M, Li H, Mukherjee S, Manfredi JJ, Gu W. Robust p53 stabilization is dispensable for its activation and tumor suppressor function. Cancer Res 2021;81:935–44.
37. Simeonova I, Jaber S, Draskovic I, Bardot B, Fang M, Bouarich-Bourimi R, et al. Mutant mice lacking the p53 C-terminal domain model telomere syndromes. Cell Rep 2013;3:2046–58.
38. Hamard PJ, Barthelery N, Hogstad B, Mungamuri SK, Tonnessen CA, Carvajal LA, et al. The C terminus of p53 regulates gene expression by multiple mechanisms in a target- and tissue-specific manner in vivo. Genes Dev 2013;27:1868–85.
39. Liu K, Lin FT, Graves JD, Lee YJ, Lin WC. Mutant p53 perturbs DNA replication checkpoint control through TopBP1 and Treslin. Proc Natl Acad Sci USA 2017;114:E3766-75.
40. Maya-Mendoza A, Moudry P, Merchut-Maya JM, Lee M, Strauss R, Bartek J. High speed of fork progression induces DNA replication stress and genomic instability. Nature 2018;559:279–84.
41. Techer H, Koundrioukoff S, Azar D, Wilhelm T, Carignon S, Brison O, et al. Replication dynamics: biases and robustness of DNA fiber analysis. J Mol Biol 2013;425:4845–55.
42. D'Angiolella V, Donato V, Forrester FM, Jeong YT, Pellacani C, Kudo Y, et al. Cyclin F–mediated degradation of ribonucleotide reductase M2 controls genome integrity and DNA repair. Cell 2012;149:1023–34.
43. Poyurovsky MV, Katz C, Laptenko O, Beckerman R, Lokshin M, Ahn J, et al. The C terminus of p53 binds the N-terminal domain of MDM2. Nat Struct Mol Biol 2010;17:982–9.
44. Giansanti C, Manzini V, Dickmanns A, Dickmanns A, Palumbieri MD, Sanchi A, et al. MDM2 binds and ubiquitinates PARP1 to enhance DNA replication fork progression. Cell Rep 2022;39:110879.
45. Kruger A, Stier A, Fischbach A, Burkle A, Hauser K, Mangerich A. Interactions of p53 with poly(ADP-ribose) and DNA induce distinct changes in protein structure as revealed by ATR-FTIR spectroscopy. Nucleic Acids Res 2019;47:4843–58.
46. Azarm K, Smith S. Nuclear PARPs and genome integrity. Genes Dev 2020;34:285–301.
47. Rudolph J, Roberts G, Luger K. Histone parylation factor 1 contributes to the inhibition of PARP1 by cancer drugs. Nat Commun 2021;12:736.
48. Fields S, Jang SK. Presence of a potent transcription activating sequence in the p53 protein. Science 1990;249:1046–8.
49. Iwabuchi K, Bartel PL, Li B, Marraccino R, Fields S. Two cellular proteins that bind to wild-type but not mutant p53. Proc Natl Acad Sci USA 1994;91:6098–102.
50. Gobert C, Skladanowski A, Larsen AK. The interaction between p53 and DNA topoisomerase I is regulated differently in cells with wild-type and mutant p53. Proc Natl Acad Sci USA 1999;96:10355–60.
51. Montero J, Dutta C, van Bodegom D, Weinstock D, Letai A. p53 regulates a non-apoptotic death induced by ROS. Cell Death Differ 2013;20:1465–74.
52. Wiman KG. p53 talks to PARP: the increasing complexity of p53-induced cell death. Cell Death Differ 2013;20:1438–9.